

PACS numbers: 42.55.Px; 42.60.Mi; 42.40.Eq; 42.81.QB
DOI: 10.1070/QE2013v043n09ABEH015155

Theoretical study of low-frequency noise and amplitude–frequency characteristics of a semiconductor laser with a fiber Bragg grating

V.D. Kurnosov, K.V. Kurnosov

Abstract. **Using the rate equations for the density of photons and charge carriers, we have studied the amplitude low-frequency noise of a fibre Bragg grating semiconductor laser. The calculations rely on two versions of the rate equation for the carriers, characterised by the presence of the optical confinement coefficient for the term, which takes into account the rate of stimulated recombination. It is shown that the relative noise intensity, which is calculated by using the rate equation for the carriers without optical confinement, agrees better with the experimental results. The calculation of the amplitude–frequency characteristics (AFCs) has shown that it is impossible to give preference to any one of these systems, since the AFCs for the two versions of the rate equations for the carriers coincide.**

Keywords: *semiconductor laser, fibre Bragg grating, low-frequency noise, amplitude–frequency characteristic.*

1. Introduction

Pumping and detecting a reference quantum transition of caesium frequency standards require highly stable single-frequency lasers.

Zhuravleva et al. [1] proposed a special design of a single-frequency laser with a fibre Bragg grating (FBG). The laser diode (LD) and FBG were mounted on two separate thermoelectric coolers, which permitted independent tuning of the wavelength to the D_2 line of caesium by changing the LD or FBG temperature. Zhuravleva et al. [2] presented a model for calculating the FBG LD characteristics, and Ivanov et al. [3] calculated the spectral characteristics of this system.

Zholnerov et al. [4] demonstrated experimentally that the discontinuities in the light–current characteristics are correlated with discontinuities in the spectral characteristics upon switching radiation both in the modes of the external cavity and in the modes of the LD. Calculations showed that the discontinuities in the light–current and spectral characteristics can be obtained by taking into account the heating of the active region of the LD due to the Joule heat and the output power coupled out from the laser cavity.

One of the main parameters of the laser, which determines the signal-to-noise ratio of the atomic beam tube (ABT), is the low-frequency amplitude noise of the laser.

V.D. Kurnosov, K.V. Kurnosov OJSC M.F. Stel'makh Polyus Research Institute, ul. Vvedenskogo 3/1, 117342 Moscow, Russia;
e-mail: mail@dilas.ru, webeks@mail.ru

Received 11 February 2013; revision received 21 May 2013
Kvantovaya Elektronika **43** (9) 828–837 (2013)
Translated by I.A. Ulitkin

The laser noise is studied based on the analysis of the rate equations. Thus, if the calculation of the photon density customary relies on the use of the gain G multiplied by the optical confinement coefficient Γ_a, the rate equation for the carrier density has two versions, including the term $\Gamma_a GS$ [5–8], or the term GS [9, 10] [S is the density of photons in the cavity; see below equations (1), (2a) and (2b)]. Since the radiation power at the LD output is independent of the employed system of the rate equations, different forms of the equations for the carriers lead to a different density of photons in the cavity. Because the noise is determined by the value of S, it is necessary to analyse the behaviour of the noise in accordance with the system of the rate equations in question and then to compare the results obtained with the experiment.

Bogatov [11], in the framework of the quasi-monochromatic field with a slowly varying amplitude and phase, found the spectral distribution of the laser power fluctuations and spectral distribution of the electron density fluctuations in the active region.

Zholnerov et al. [12] studied experimentally the amplitude noise of FBG LDs. The main feature of the plots shown in the paper is that the discontinuities in the relative intensity noise (RIN) characteristics are correlated with discontinuities in the light–current characteristic. In this case, the maximum noise is observed for the current varying from 70 to 73 mA (corresponding to switching on the radiation in the modes of the laser diode) when simultaneous lasing of two modes with approximately equal amplitudes takes place.

The aim of this paper is to calculate, based on the model [2], the FBG LD noise characteristics using the results obtained in [5–8].

2. Design equations

In accordance with the above provisions, the rate equations for the two variants can be written in the form (1) and (2a) or (1) and (2b):

$$\frac{\mathrm{d}S_{1i}}{\mathrm{d}t} = \left(F_{1i}G_i - \frac{1}{\tau_i}\right)S_{1i} + \beta F_{1i}R_{\mathrm{sp}} + F_i(t), \tag{1}$$

$$\frac{\mathrm{d}n_{\mathrm{a}}}{\mathrm{d}t} = \frac{I}{eV_{\mathrm{a}}} - A_{\mathrm{n}}n_{\mathrm{a}} - R_{\mathrm{sp}} - \sum G_i S_{1i} + F_{\mathrm{e}}(t), \tag{2a}$$

$$\frac{\mathrm{d}n_{\mathrm{a}}}{\mathrm{d}t} = \frac{I}{eV_{\mathrm{a}}} - A_{\mathrm{n}}n_{\mathrm{a}} - R_{\mathrm{sp}} - \frac{1}{\Gamma_{\mathrm{a}}}\sum G_i S_{1i} + F_{\mathrm{e}}(t), \tag{2b}$$

where S_{1i} is the photon density in the ith mode of the LD cavity; n_{a} is the carrier density; β is the coefficient taking into account the contribution of spontaneous emission to the lasing

mode; $F_i(t)$ and $F_e(t)$ are the Langevin noise operators; $A_n n_a$ is the rate of nonradiative recombination of the carriers; V_a is the volume of the active region; and I is the pump current.

The lifetime of a photon in the FBG LD cavity is

$$\tau_i = \left[c_0\left(\frac{F_{1i}}{n_{1i}}\alpha_{1\Sigma} + \frac{F_{2i}}{n_2}\alpha_{2\Sigma} + \frac{F_{3i}}{n_3}\alpha_{3\Sigma} + \frac{F_{Bi}}{n_B}\alpha_{B\Sigma}\right)\right]^{-1}, \quad (3)$$

where c_0 is the speed of light in vacuum. The coefficients F_{ji} determine the relative distribution of the photon density in the constituent parts of the laser cavity: $F_{1i} = V_1 S_{1i}/V_\Sigma S_i$, $F_{2i} = V_2 S_{2i}/V_\Sigma S_i$, $F_{3i} = V_3 S_{3i}/V_\Sigma S_i$, $F_{Bi} = V_B S_{Bi}/V_\Sigma S_i$, $\sum F_{ji} = 1$, $V_\Sigma = V_1 + V_2 + V_3 + V_B$ ($V_1 = V_a/\Gamma_a$, V_2, V_3 and V_B are the volumes of the constituent parts of the cavity). The averaged photon density S_i and volumes V_1, V_2, V_3 and V_B are determined by formulas (14) and the coefficients F_{ji} and optical losses $\alpha_{j\Sigma}$ ($j = 1, 2, 3$ and B) in the constituent parts of the cavity by expressions (18) and (20) from paper [2].

The rate of spontaneous recombination of the carriers is

$$R_{sp} = Bn_a^2 = n_a/\tau_{sp}, \quad (4)$$

where $\tau_{sp} = (Bn_a)^{-1}$ is the carrier lifetime upon spontaneous recombination, and B is a coefficient that is considered constant.

The linearisation of the gain maximum (22) from [2] allowed us to obtain an expression for the gain, which depends on the carrier density in the active region of the laser:

$$G_i = Q_i(n_a D_i - n_{a0}), \quad (5)$$

where

$$Q_i = \frac{c_0\Gamma_a}{n_{1i}}\frac{dg}{dn_a};\ D_i = 1 - \left[\frac{2(E_i - E_g)}{\Delta E_g}\right]^2;$$

dg/dn_a is the differential gain; $E_i = 1.24/\lambda_i$ (λ_i is the radiation wavelength of the ith mode in micrometres); E_g is the band gap; $\Delta E_g = 0.18$ eV is the width of the gain spectrum; $n_{a0} = 1.75\times10^{18}$ cm^{-3} is the carrier density at which the gain is equal to zero.

For E_g we derive the expression

$$E_g = E_0 - 5.4\times10^{-4}T^2/(204 + T) - 2k_g n_a^{1/3}, \quad (6)$$

where $E_0 = 1.63$ eV (as determined by the band gap of a bulk semiconductor with the quantisation levels in the valence band and the conduction band taken into account); and k_g is a coefficient which takes account of the change in the band gap due to filling by the carriers.

We are interested in the spectral and power characteristics of the laser when the pump current of the LD changes at a fixed temperature T_0 of the contact plate with the LD mounted and at a fixed FBG temperature T_B (T_0 and T_B are maintained constant through the use of two coolers).

The temperature of the active region of LD can be written as

$$T = T_0 + \delta T. \quad (7)$$

Change in the temperature of the active region as a function of the pump current I flowing through the LD and output power P_1 coupled from the LD cavity can be represented as [4]

$$\delta T = R_T(U_{pn}I + I^2R_d - 2P_1), \quad (8)$$

where R_T is the thermal resistance of the LD; U_{pn} is the voltage at the p–n transition; and R_d is the dynamic resistance of the LD.

With $T_0 \gg \delta T$ taken into account (we assume that $T_0 = 293$ K and $\delta T \leqslant 10$ K [4]), the expression for the D_i in formula (5) can be linearised with respect to temperature T_0:

$$D_i(T, n_a) = D_i(T_0, n_a) + \left.\frac{dD_i}{dT}\right|_{T=T_0}\delta T$$
$$= D_{i0}(T_0, n_a) + A_{Ti}P_1, \quad (9)$$

where

$$D_{i0}(T_0, n_a) = D_i(T_0, n_a) + \frac{8[E_i - E_g(T_0, n_a)]}{\Delta E_g^2}\left.\frac{dE_g}{dT}\right|_{T=T_0}$$
$$\times R_T(U_{pn}I + I^2R_d);$$
$$A_{Ti} = -\frac{16[E_i - E_g(T_0, n_a)]}{\Delta E_g^2}\left.\frac{dE_g}{dT}\right|_{T=T_0}R_T. \quad (10)$$

According to (9) and (10), the gain (5) can be represented in the form

$$G_i(T, n_a) = Q_i\{n_a[D_{i0}(T_0, n_a) + A_{Ti}P_1] - n_{a0}\}, \quad (11)$$

where P_1 is the emission power coupled out through the LD facet.

When account is taken of the active region heating calculated using formula (8), the gain depends on the power P_1, and we can introduce the nonlinearity coefficient

$$\varepsilon_i = -\frac{n_a A_{Ti}P_1}{n_a D_{i0}(T_0, n_a) - n_{a0}}. \quad (12)$$

For system (1) and (2a) we have [2]

$$P_1 = A_{power}\sum_i S_{1i}, \quad (13)$$

where $A_{power} = h\nu_B v_{gr}S_{cs}(1 - R_1)$; $h\nu_B = 1.24q/\lambda_B$; λ_B is the Bragg wavelength expressed in micrometres; q is the electron charge; v_{gr} is the group velocity; R_1 is the reflectance of the LD facet; and S_{cs} is the cross-section area of the active region of the LD.

The refractive index of the active region of the LD can be written as

$$n_{1i} = n_{10}\left[1 + \frac{1}{n_{10}}\frac{\partial n_1}{\partial\lambda}(\lambda_i - \lambda_B) + \frac{1}{n_{10}}\frac{\partial n_1}{\partial T}(T - T_0)\right], \quad (14)$$

where n_{10} is the refractive index of the active region of the LD for $\lambda = \lambda_B$ and $T = T_0$. The refractive indices n_2 and n_B depend only on the wavelength and are given by (13) and (14) in [4].

In studying the noise characteristics we linearised the rate equation for the carrier density relative to the stationary value of $\bar{n}_a$, by assuming that $n_a = \bar{n}_a + \Delta n_a$. Therefore, we linearise the expression for D_i, which enters the gain (5):

$$D_i(T, n_a) = D_i(T, \bar{n}_a) + A_{gi}\Delta n_a$$
$$= D_{i0}(T, \bar{n}_a) + A_{Ti}P_1 + A_{gi}\Delta n_a, \quad (15)$$

where

$$A_{gi} = \frac{\mathrm{d}D_i}{\mathrm{d}n_a}\Big|_{n_a=\bar{n}_a} = \frac{8[E_i - E_g(T,\bar{n}_a)]}{\Delta E_g^2}\frac{\mathrm{d}E_g}{\mathrm{d}n_a}\Big|_{n_a=\bar{n}_a},$$

$$\frac{\mathrm{d}E_g}{\mathrm{d}n_a} = -\frac{2}{3}k_g(\bar{n}_a)^{-2/3},\ E_g(T,\bar{n}_a) = E_g(T_0,\bar{n}_a) + \frac{\mathrm{d}E_g}{\mathrm{d}T}\Big|_{T=T_0}\delta T.$$

The gain (5) with Eqn (15) taken into account can be written in the form

$$G_i(T,n_a) = \bar{G}_i(T,\bar{n}_a) + \Delta G_i(T,\bar{n}_a), \tag{16}$$

where $G_i = \bar{G}_i(T,\bar{n}_a) = Q_i\{\bar{n}_a[D_{i0}(T_0,\bar{n}_a) + A_{Ti}P_1] - \bar{n}_{a0}\}$ and $\Delta G_i(T,\bar{n}_a) = Q_i[D_{i0}(T_0,\bar{n}_a) + A_{Ti}P_1 + A_{gi}\bar{n}_a]\Delta n$.

3. Calculation of the noise characteristics in the case of a single mode

By substituting $n_a = \bar{n}_a + \Delta n_a$ and $S_{1p} = \bar{S}_{1p} + \Delta S_{1p}$ in equations (1) and (2a) or (2b), we obtain the equations for stationary values and increments. The values of $\bar{n}_a$ and $\bar{S}_{1p}$ were calculated from the combined solution of stationary equations (1), (2a) or (2b) and characteristic equation (6) from [2]. For a given pump current we determined the set of the modes that can propagate through the FBG LD system. For each mode we calculated the photon density, selected the maximum value to which the subscript p ($\bar{S}_{1p}$) is assigned. The radiation power was calculated using formula (13).

For the increments we obtain the expressions [5–8]

$$\begin{aligned}
\mathrm{j}\omega\Delta n_a(\omega) &= A_{1p}\Delta n_a(\omega) + A_{2p}\Delta S_{1p}(\omega) + F_e,\\
\mathrm{j}\omega\Delta S_{1p}(\omega) &= A_{3p}\Delta n_a(\omega) + A_{4p}\Delta S_{1p}(\omega) + F_p,\\
S_{1p}(t) &= \bar{S}_{1p} + \Delta S_{1p}(t) = \bar{S}_{1p} + \int_{-\infty}^{\infty}\Delta S_{1p}(\omega)\exp(\mathrm{j}\omega t)\,\mathrm{d}t,\\
n_a(t) &= \bar{n}_a + \Delta n_a(t) = \bar{n}_a + \int_{-\infty}^{\infty}\Delta n_a(\omega)\exp(\mathrm{j}\omega t)\,\mathrm{d}t.
\end{aligned} \tag{17}$$

Expressions (17) allow us to determine $\Delta S_{1p}(\omega)$ for system (1) and (2a) in the form

$$\Delta S_{1p}(\omega) = T_p(\omega)F_p + T_e(\omega)F_e, \tag{18}$$

where $T_p(\omega) = (\mathrm{j}\omega - A_{1p})/Y(\omega)$ and $T_e(\omega) = A_{3p}/Y(\omega)$, $Y(\omega) = (\mathrm{j}\omega - A_{1p})(\mathrm{j}\omega - A_{4p}) - A_{2p}A_{3p}$,

$$\begin{aligned}
A_{1p} &= -A_n - 2B\bar{n}_a - Q_p\bar{S}_{1p}(D_{p0} + A_{Tp}P_1 + A_{gp}\bar{n}_a),\\
A_{2p} &= -Q_p[\bar{n}_a(D_{p0} + A_{Tp}P_1) - n_{a0}],\\
A_{3p} &= F_{1p}\beta B2\bar{n}_a + F_{1p}Q_p\bar{S}_{1p}(D_{p0} + A_{Tp}P_1 + A_{gp}\bar{n}_a),\\
A_{4p} &= -F_{1p}\beta B\bar{n}_a^2/\bar{S}_{1p}.
\end{aligned} \tag{19}$$

The relative intensity noise (RIN) in a single frequency band may be written in the form

$$\mathrm{RIN} = 10\lg\frac{\langle\Delta S_{1p}(\omega)\Delta S_{1p}^*(\omega)\rangle}{\bar{S}_{1p}^2} = 10\lg\left[\frac{F_p^2|T_p|^2 + F_e^2|T_e|^2 + 2F_pF_e\,\mathrm{Re}(T_pT_e^*)}{\bar{S}_{1p}^2}\right], \tag{20}$$

where ΔS_{1p}^* is the complex conjugate value.

The rms noise power in a single frequency band is defined as

$$P_{\mathrm{noise}} = \sqrt{\langle\Delta P_1^2\rangle} = A_{\mathrm{power}}\sqrt{\langle\Delta S_{1p}(\omega)\Delta S_{1p}^*(\omega)\rangle}. \tag{21}$$

For system (1) and (2b) in the expressions for the coefficients A_{1p} and A_{2p} (19), we should replace Q_p by Q_p/Γ_a and multiply the value of A_{power} in formula (21) by $1/\Gamma_a$.

For Langevin noise sources we will use the expressions obtained in [6]. For the system of equations (1) and (2a) they can be written in the form

$$F_p^2 = \frac{1}{V_1}\left\{F_{1p}Q_p[\bar{n}_a(D_{p0} + A_{Tp}P_1) + n_{a0}]\bar{S}_{1p} + \frac{\bar{S}_{1p}}{\tau_p} + F_{1p}\beta B\bar{n}_a^2\right\}, \tag{22}$$

$$F_e^2 = \frac{1}{V_a}\left\{\frac{I}{eV_a} + A_n n_a + Bn_a^2 + Q_p[\bar{n}_a(D_{p0} + A_{Tp}P_1) + n_{a0}]\bar{S}_{1p}\right\}, \tag{23}$$

$$F_pF_e = -\frac{1}{V_1}\{F_{1p}Q_p[\bar{n}_a(D_{p0} + A_{Tp}P_1) + n_{a0}]\bar{S}_{1p} + F_{1p}\beta B\bar{n}_a^2\}. \tag{24}$$

For the system of equations (1) and (2b) formulas (22) and (24) will remain unchanged, and in equation (23) Q_p should be replaced by Q_p/Γ_a.

The coefficients necessary for the calculations are borrowed from papers [2, 4]. The dependences shown in Figs 1–4 are calculated for $R_T = 38$ K W^{-1}, and in Fig. 5 – for $R_T = 50$ K W^{-1}. The dependences calculated for the system of equations (1) and (2b) are shown in Figs 1a–c, and for system (1) and (2a) – in Figs 1d, e. It is found that the $P_1(I)$ dependences for the two systems are identical and the $S_{1p}(I)$ dependences are qualitatively similar but differ in magnitude by about two of magnitude [S_{1p} for system (1) and (2a) varies in the range $(0–8)\times10^{16}$ cm^{-3} (the curve is not shown) and system (1) and (2b) – in the range $(0–8)\times10^{14}$ cm^{-3}]. The graphs for the relative intensity noise differ from each other. For example, at $I = 60$ mA for system (1) and (2b) RIN = –150 dB Hz^{-1} (Fig. 1b), and for system (1) and (2a) RIN = –165 dB Hz^{-1} (Fig. 1d). Different is the behaviour of the $P_{\mathrm{noise}}(I)$ dependences presented in Figs 1c and 1e. By comparing the dependences for RIN and P_{noise} in Figs 1b and 1c with the experimental curves in Figs 2 and 3 from [12], we see that plots for RIN and P_{noise} in Figs 1b and 1c, by the nature of changes and the absolute value, are closer to the experimental curves than similar dependences in Figs 1d and 1e.

Thus, we can assume that the results of calculations for system (1) and (2b) correspond better to the experiment than those for system (1) and (2a).

4. Calculation of the noise characteristics in the case of two modes

For the system of equations (1) and (2a), the radiation power at the LD output in the case of two modes may be written in the form

$$P_1 = A_{\mathrm{power}}(S_{1p} + S_{1q}), \tag{25}$$

where S_{1p} and S_{1q} are photon densities in the modes p and q [for system (1) and (2b) into the right-hand side of (25) we should add the factor $1/\Gamma_a$]. As in the case of a single mode, for a given pump current we determined the set of the modes that can propagate through the FBG LD system, calculated the density of photons in the modes, selected the maximum photon density to which the subscript p is assigned. Then for

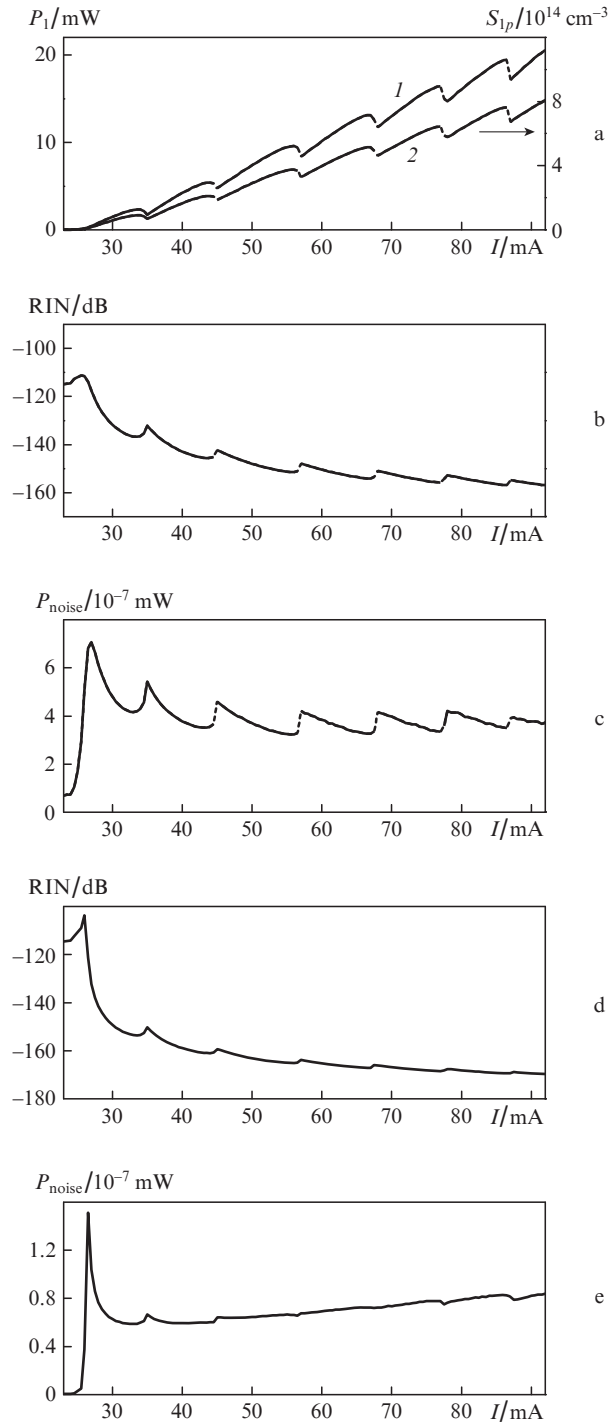

Figure 1. (a) Radiation power P_1 (*1*) and photon density S_{1p} (*2*), (b) relative intensity noise RIN and (c) P_{noise}, calculated with formula (8) taken into account for one mode by using the system of equations (1) and (2b), as well as by using the system of equations (1) and (2a)–(d) RIN, (e) P_{noise} vs. pump current. RIN and P_{noise} values are given in a single frequency band.

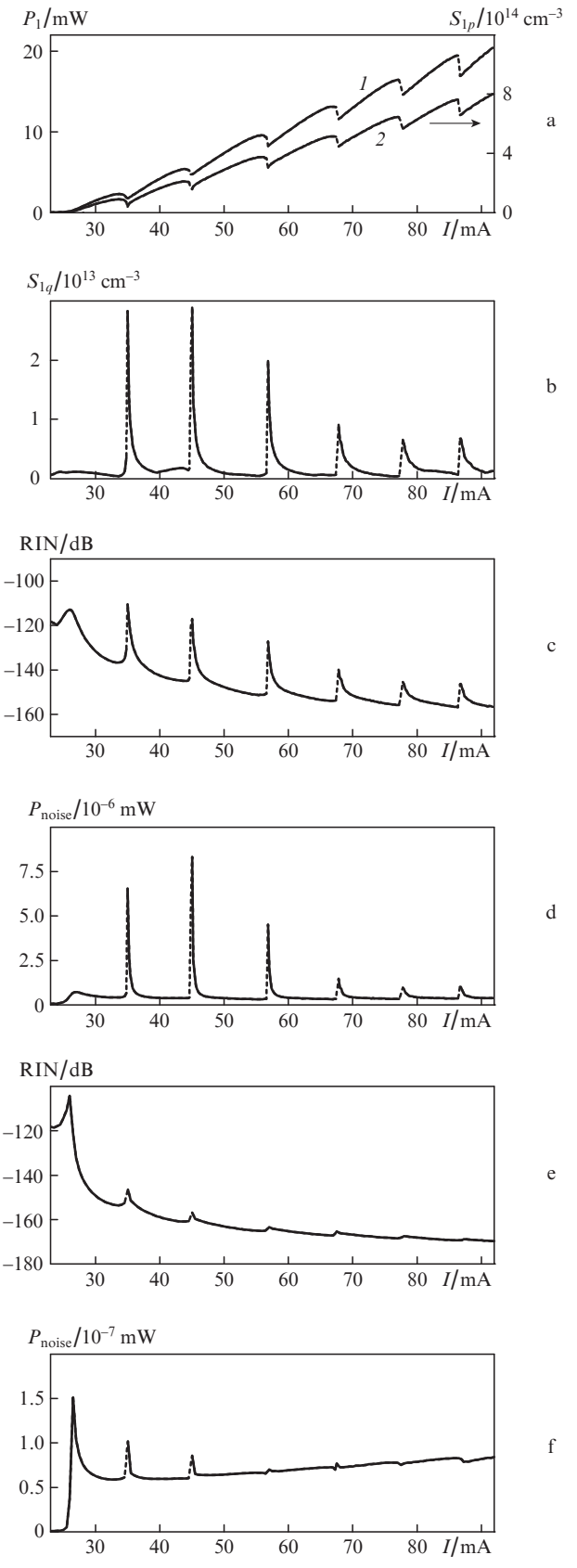

Figure 2. (a) Radiation power P_1 (*1*) and photon density in the p mode S_{1p} (*2*), (b) photon density in the q mode S_{1q}, (c) relative intensity noise RIN and (d) P_{noise}, calculated with formula (8) taken into account for two modes by using the system of equations (1) and (2b), as well as by using the system of equations (1) and (2a)–(e) RIN, (f) P_{noise} vs. pump current. RIN and P_{noise} values are given in a single frequency band.

the modes $i \neq p$ we found the maximum value of the photon density to which the subscript q is assigned. The radiation power was calculated using formula (25).

Similarly to the previous case, for the two modes we can obtain

$$\begin{aligned} j\omega\Delta n_a(\omega) &= A_1\Delta n_a(\omega) + A_{2p}\Delta S_{1p}(\omega) + A_{2q}\Delta S_{1q}(\omega) + F_e, \\ j\omega\Delta S_{1i}(\omega) &= A_3\Delta n_a(\omega) + A_{4i}\Delta S_{1i}(\omega) + F_i, \quad i = p, q. \end{aligned} \tag{26}$$

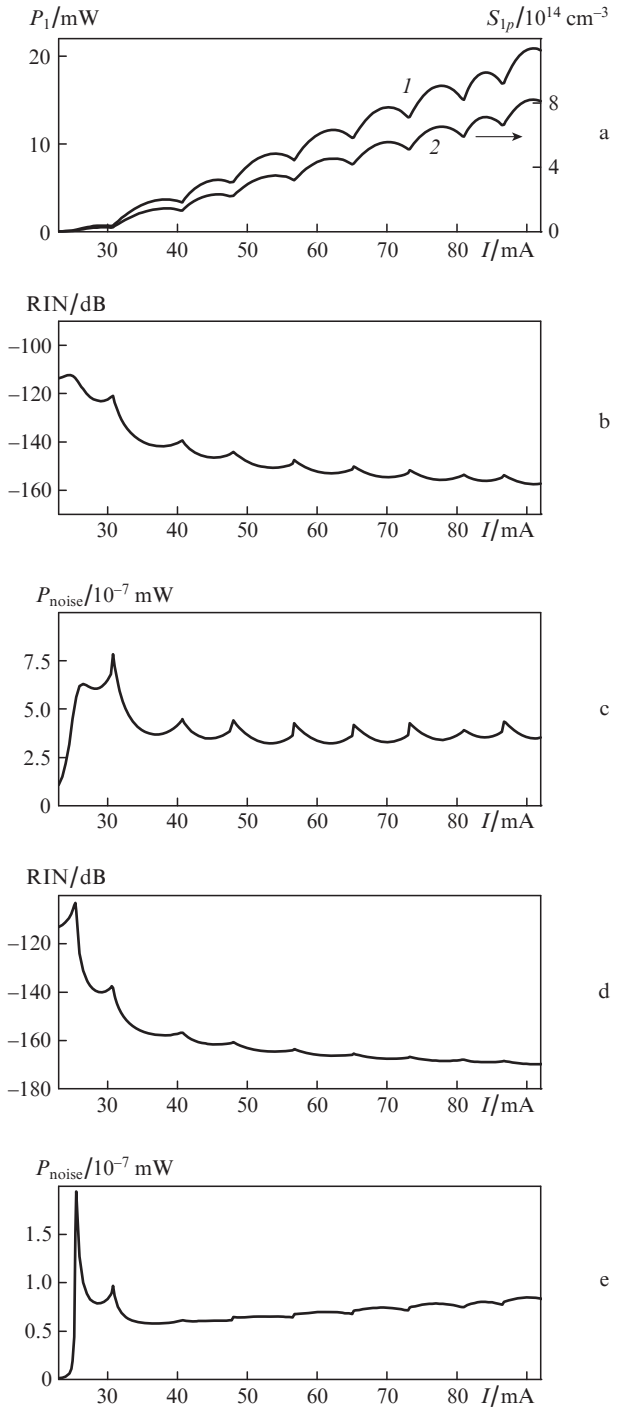

Figure 3. Pump current dependences calculated with formula (32) taken into account for one mode by using the system of (a–c) equations (1) and (2b) and (d, e) (1) and (2a). Notations are the same as in Fig. 1.

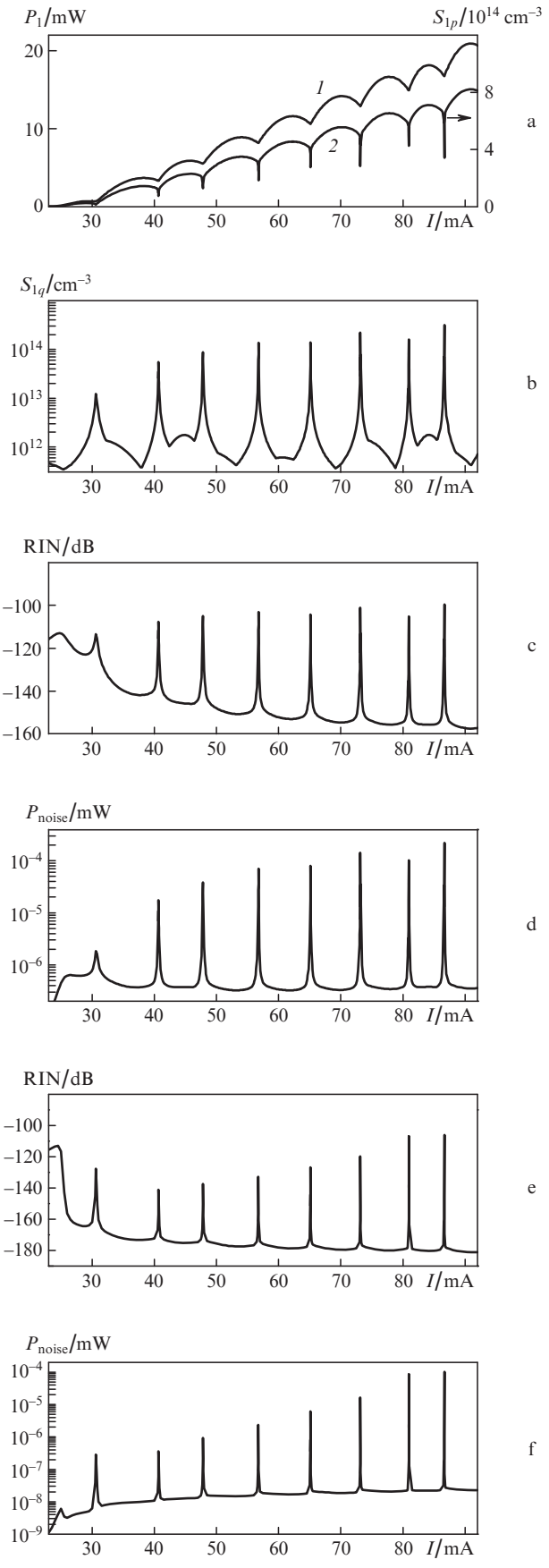

Figure 4. Pump current dependences calculated with formula (32) taken into account for two modes by using the system of (a–d) equations (1) and (2b) and (e, f) (1) and (2a). Notations are the same as in Fig. 2.

Expressions (26) allow us to determine $\Delta S_{1p}(\omega)$ in the form

$$\Delta S_{1p}(\omega) = T_{pp}(\omega)F_p + T_{pq}(\omega)F_q + T_{pe}(\omega)F_e, \quad (27)$$

where

$$T_{pp}(\omega) = \frac{1}{j\omega - A_{4p}} + \frac{A_{2p}A_{3p}(j\omega - A_{4q})}{Y_1(\omega)(j\omega - A_{4p})},$$

$$T_{pq}(\omega) = \frac{A_{3p}A_{2q}}{Y_1(\omega)},\ T_{pe}(\omega) = \frac{A_{3p}(j\omega - A_{4q})}{Y_1(\omega)}, \quad (28)$$

$$Y_1(\omega) = (j\omega - A_1)(j\omega - A_{4p})(j\omega - A_{4q}) - A_{2p}A_{3p}(j\omega - A_{4q}) - A_{2q}A_{3q}(j\omega - A_{4p}).$$

For ΔS_{1q} we obtained an equality analogous to (27) by replacing the subscript p by q. This also applies to the coefficients $T_{qq}(\omega)$, $T_{qp}(\omega)$ and $T_{qe}(\omega)$.

The coefficients in (28) have the form:

$$A_1 = -A_n - 2B\bar{n}_a - Q_p(D_{p0} + A_{Tp}P_1 + A_{gp}\bar{n}_a)\bar{S}_{1p} - Q_q(D_{q0} + A_{Tq}P_1 + A_{gq}\bar{n}_a)\bar{S}_{1p},$$

$$A_{2p} = -Q_p[\bar{n}_a(D_{p0} + A_{Tp}P_1) - n_{a0}],$$

$$A_{2q} = -Q_q[\bar{n}_a(D_{q0} + A_{Tq}P_1) - n_{a0}], \quad (29)$$

$$A_{3p} = F_{1p}Q_p(D_{p0} + A_{Tp}P_1 + A_{gp}\bar{n}_a) + F_{1p}\beta B2\bar{n}_a,$$

$$A_{3q} = F_{1q}Q_q(D_{q0} + A_{Tq}P_1 + A_{gq}\bar{n}_a) + F_{1q}\beta B2\bar{n}_a,$$

$$A_{4p} = -F_{1p}\beta B\bar{n}_a^2/\bar{S}_{1p},\ A_{4q} = -F_{1q}\beta B\bar{n}_a^2/\bar{S}_{1q}.$$

For the relative intensity noise of the mode p we have

$$\mathrm{RIN} = 10\lg\frac{\langle\Delta S_{1p}(\omega)\Delta S_{1p}^*(\omega)\rangle}{(\bar{S}_{1p} + \bar{S}_{1q})^2} = 10\lg\{[F_p^2|T_{pp}|^2 + F_q^2|T_{pq}|^2 + F_e^2|T_{pe}|^2 + 2F_pF_e\mathrm{Re}(T_{pp}T_{pe}^*) + 2F_qF_e\mathrm{Re}(T_{pq}T_{pe}^*)]/(\bar{S}_{1p} + \bar{S}_{1q})^2\}. \quad (30)$$

Langevin noise sources for F_p^2 and F_pF_e obey relationships (22) and (24). Expressions F_q^2 and F_qF_e are found from (22) and (24) by replacing the subscript p by q. The expression for F_e^2 takes the form

$$F_e^2 = \frac{1}{V_a}\left\{\frac{I}{eV_a} + A_n n_a + Bn_a^2 + Q_p[\bar{n}_a(D_{p0} + A_{Tp}P_1) + n_{a0}]\bar{S}_{1p} + Q_q[\bar{n}_a(D_{q0} + A_{Tq}P_1) + n_{a0}]\bar{S}_{1q}\right\}. \quad (31)$$

In the case of two modes the calculated dependences for system (1) and (2b) are presented in Figs 2a–d, and for system (1) and (2a) – in Figs 2e and 2f. The calculation shows that the $P_1(I)$ dependences for systems (1) and (2b) and (1) and (2a) coincide. The photon density in the mode p for system (1) and (2a) is two orders of magnitude greater than for system (1) and (2b), whereas the photon densities in the mode q are approximately equal to each other. The relative intensity noise of system (1) and (2b) is significantly higher than that of (1) and (2a). Thus, for the 60-mA current the RIN in the first case is –150 dB Hz^{-1} (Fig. 2c), and in the second case, RIN = –165 dB Hz^{-1} (Fig. 2e) (as in the case of a single mode). The value of P_{noise} in Fig. 2f is significantly lower than in Fig. 2d. This is explained by the fact that the density of photons in the p mode S_{1p} for system (1) and (2a) is two orders of magnitude greater than for system (1) and (2b), whereas the photon densities in the q mode S_{1q} are approximately equal to each other.

The density of photons in the p mode S_{1p} is nonlinear and increases with increasing pump current. The density of photons in the q mode S_{1q} decreases with increasing I, which leads to a decrease in the amplitude noise. For a current corresponding to switching on from one mode of the LD or FBG to the other, it is impossible to obtain in calculations approximately equal amplitudes S_{1p} and S_{1q}. Thus, taking into account the heating of the active region of the LD defined by formula (8), the 'strong' mode p suppresses the 'weak' mode q, and generation of these modes with approximately equal amplitudes is impossible.

5. Characteristics of FBG LDs without taken into account the radiation power coupled out of the laser cavity

To take account of the heating of the active region of the LD, Eliseev [13] proposed to use the expression

$$\delta T = R_T[U_{pn}I(1 - \eta) + I^2R_g], \quad (32)$$

which differs from (8) by the absence of the term $2P_1$ – the radiation power coupled out of the LD cavity. Reduced heating of the active region in this case is taken into account by introducing a constant efficiency coefficient η. In the calculations we assumed $\eta = 0.25$.

The same dependences for a single mode as in Fig. 1, calculated with formula (32) taken into account, are shown in Fig. 3.

One can see that the $P_1(I)$ and $S_{1p}(I)$ dependences in Fig. 3a do not have discontinuities inherent in these dependences (Fig. 1a). The absence of discontinuities is inherent in other characteristics, shown in Fig. 3. The plots of the RIN(I) dependences for both systems differ from each other. For example, at I = 58 mA the RIN for system (1) and (2b) is 15 dB less than for system (1) and (2a). The $P_{noise}(I)$ dependences (Figs 3c and 3e) differ not only in magnitude but also in form.

The situation changes dramatically when two modes are considered (Fig. 4). The plots of $P_1(I)$ are the same for both systems. The density of photons in the mode $p(q)$ for system (1) and (2a) is almost two orders of magnitude (one order of magnitude) higher than that for system (1) and (2b).

Comparison of $P_1(I)$ and $S_{1p}(I)$ dependences in Fig. 4a with similar dependences in Fig. 2a shows that in the case of two modes these characteristics have no discontinuities. The $S_{1q}(I)$ dependence (Fig. 4b) has no discontinuities and increases with increasing pump current (in contrast to the behaviour of $S_{1q}(I)$ in Fig. 2b). A similar behaviour pattern is inherent in the RIN(I) and $P_{noise}(I)$ dependences (Figs 4c, e and Figs 4d, f) – noise increases with increasing pump current.

The difference in the behaviour of the characteristics is due to the fact that when formula (32) is used in calculations,

there can simultaneously exist two modes with approximately equal amplitudes; however, this is impossible when use is made of formula (8).

6. Calculation of the RIN for the FBG LD system in the low-frequency region

Calculations show that at low frequencies (down to 60 kHz) it is impossible to achieve the coincidence of experimental and theoretical RIN dependences, obtained from formulas (20) or (30). Therefore, usually Hooge's hypothesis [14] is used in considering low-frequency noises. Garmash et al. [15] noted that the presence of such noise as $1/f$ changes the correlation ratio for F_e^2 so that the low-frequency component of the spectral noise density for the system of rate equations (1) and (2b) can be written in the form

$$F_e^2 = \frac{1}{V_a}\left\{\frac{I}{eV_a} + A_n n_a + Bn_a^2 + Q_p \frac{1}{\Gamma_a}[\bar{n}_a(D_{p0} + A_{Tp}P_1) + n_{a0}]\bar{S}_{1p} + \frac{\alpha_H n_a}{\omega\tau_e^2}\right\}. \quad (33)$$

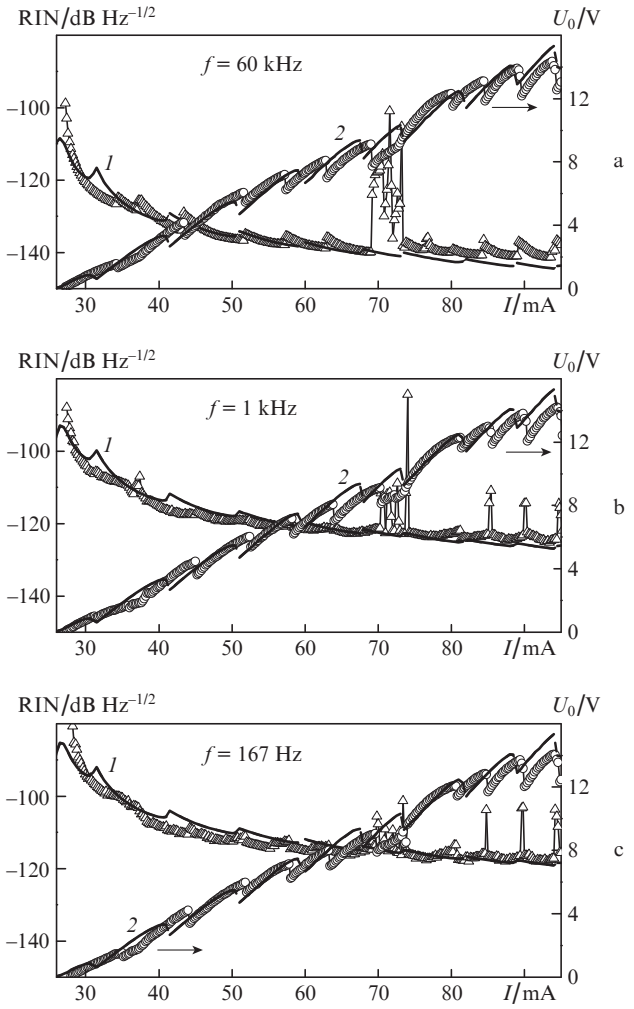

Figure 5. Pump current vs. relative intensity noise (*1*) and voltage U_0 (*2*) proportional to the LD radiation power for frequencies f = (a) 60, (b) 1 and (c) 0.167 kHz in the case of a single mode. The calculations are performed for the system of equations (1) and (2b). The experimental dependences are given by empty circles and triangles.

In this case, relations (22) and (24) remain unchanged. Here α_H is the Hooge constant, and $\tau_e = (A_n + Bn_a)^{-1}$ is the carrier lifetime in view of non-radiative and spontaneous recombination. Calculations show that for theoretical and experimental dependences to coincide we should have $\alpha_H = 0.8$.

To match the calculated and experimental results, we will take into account that in a single frequency band

$$\mathrm{RIN} = 10\lg\frac{\langle\Delta S_{1p}^2\rangle}{\bar{S}_{1p}^2} = 10\lg\frac{\langle\Delta P_1^2\rangle}{P_1^2}\left(\frac{\mathrm{dB}}{\mathrm{Hz}}\right) = 20\lg\frac{U_{\mathrm{noise}}}{U_0}\left(\frac{\mathrm{dB}}{\sqrt{\mathrm{Hz}}}\right), \quad (34)$$

where $U_0 = \eta_{pd}R_{pd}P_1$; $U_{\mathrm{noise}} = \sqrt{\langle\Delta U_{\mathrm{noise}}^2\rangle} = \eta_{pd}R_{pd}\sqrt{\langle\Delta P_1^2\rangle}$; η_{pd} is the photodiode sensitivity; and R_{pd} is the load resistance in the photodiode circuit [16]. The theoretical curves shown in Fig. 5 are calculated at $\eta_{pd} = 0.6$ A W^{-1} and $R_{pd} = 1$ kΩ.

Figure 5a shows the dependence of the voltage U_0 and RIN on the pump current at $f = 60$ kHz for a single mode of system (1) and (2b) [the RIN(I) dependence is calculated using formula (34)]. Figures 5b and c present similar dependences for the frequencies f = 1 and 0.167 kHz. One can see that the theoretical and experimental dependences coincide in the order of magnitude. However, the calculations do not show a sharp increase in the noise level in the current range from 70 to 73 mA, corresponding to switching on the radiation in the LD modes, and an increase in the noise in the current range from 80 to 95 mA.

7. Calculation of the amplitude–frequency characteristics

Consider two systems of rate equations (1), (2a) and (1), (2b) with the active heating region of the LD taken into account which is defined by formula (8) (excluding Langevin noise operators). We assume that the pump current I has a constant, $\bar{I}$, and a variable component, $\Delta i(\omega)$,

$$I = \bar{I} + \Delta i(\omega)\exp(j\omega t), \quad (35)$$

which leads to modulation of both the carrier density and the photon density:

$$n_a = \bar{n}_a + \Delta n_a(\omega)\exp(j\omega t), \quad S_{1p} = \bar{S}_{1p} + \Delta S_{1p}(\omega)\exp(j\omega t), \quad (36)$$

where ω is the modulation frequency; and $\bar{n}_a$, $\bar{S}_{1p}$ are the constants of the carrier and photons densities.

Single-mode approximation. By substituting (35) and (36) into the system of equations (1) and (2a), we obtain the equation for the stationary values and increments. As previously, we use the p mode, for which the photon density is maximal. The wavelength λ_p corresponds to this mode. The radiation power was calculated using formula (13).

For increments we obtain the equations:

$$j\omega\Delta n_a(\omega) = \frac{\Delta i(\omega)}{eV_a} + A_{1p}\Delta n_a(\omega) + A_{2p}\Delta S_{1p}(\omega), \quad j\omega\Delta S_{1p}(\omega) = A_{3p}\Delta n_a(\omega) + A_{4p}\Delta S_{1p}(\omega), \quad (37)$$

which allow one to define the relationship

$$\frac{\Delta S_{1p}(\omega)}{\Delta i(\omega)} = \frac{A_{3p}}{eV_{\rm a}\,Y(\omega)}, \tag{38}$$

where the coefficient $Y(\omega)$ and its coefficients A_{1p}, A_{2p}, A_{3p} and A_{4p} are determined by expressions (19).

In view of (38) the normalised AFC can be written in the form

$$M_1(\omega) = 10\lg\left[\frac{\Delta S_{1p}(\omega)/\Delta S_{1p}(0)}{\Delta i(\omega)/\Delta i(0)}\right]^2 = 10\lg\left[\frac{\omega_0^4}{(\omega_0^2-\omega^2)^2-(\omega\mu)^2}\right], \tag{39}$$

$$\omega_0^2 = A_{1p}A_{4p} - A_{2p}A_{3p},\ \mu = -(A_{1p}+A_{4p}). \tag{40}$$

Figure 6 shows the dependences of the radiation power P_1, wavelength λ_p, photon lifetime τ_p and relaxation oscillation frequency ω_0^2 on the pump current for the lengths of FBG fibres L_2 = 7.6 and 1.0 mm. The photon lifetime was calculated using formula (3). It can be seen that all the characteristics have discontinuities that correlate with discontinuities in the light–current and spectral characteristics. A comparison of the curves shown in Figs 6a and b shows that a decrease in the fibre length from 7.6 to 1.0 mm increases the range of continuous tuning of the radiation power and wavelength, decreases the photon lifetime and increases the frequency ω_0^2. According to the calculations for a given pump current the AFCs coincide (with an error of less than 3%) for both systems. The coincidence of the AFCs can be explained if in formula (40) we write the expressions for the coefficients A_{1p}, A_{2p}, A_{3p} and A_{4p} in the form of (19). Then, we obtain

$$\omega_0 = 2\pi f_0 \approx \left[\frac{c_0\Gamma_{\rm a}}{n_1}\frac{{\rm d}g}{{\rm d}n_a}\frac{1}{\tau_p}\frac{P_1}{A_{\rm power}} + (A_{\rm n}+2Bn_{\rm a})\frac{F_{1p}\beta Bn_{\rm a}^2}{S_{1p}}\right]^{1/2}. \tag{41}$$

Calculations show that in the developed generation regime, the last term in (41) can be neglected; therefore, ω_0 is determined by the radiation power P_1, which, in turn, is independent of the chosen system (1), (2a) or (1), (2b).

The dependence $\omega_0^2(I)$ (Fig. 6a), as the dependences of $P_1(I)$ and $\lambda(I)$, has discontinuities and hence the performance of the FBG LD depends on the selected operating point and may decrease with increasing I [points A and B on curve (4); Fig. 6a).

Two-mode approximation. Following the procedure described in Section 4, we selected the modes with subscripts p and q (with wavelengths λ_p and λ_q). The radiation power was calculated using formula (25); P_1 and radiation wavelengths λ_p and λ_q are shown in Fig. 7.

For the increments we obtain

$$\begin{aligned} {\rm j}\omega\Delta n_{\rm a}(\omega) &= \frac{\Delta i(\omega)}{eV_{\rm a}} + A_1\Delta n_{\rm a}(\omega) + A_{2p}\Delta S_{1p}(\omega) + A_{2q}\Delta S_{1q}(\omega), \\ {\rm j}\omega\Delta S_{1i}(\omega) &= A_3\Delta n_{\rm a}(\omega) + A_{4i}\Delta S_{1i}(\omega),\ i = p, q. \end{aligned} \tag{42}$$

Expressions (42) allow us to determine the ratio

$$\frac{\Delta S_{1p}(\omega)+\Delta S_{1q}(\omega)}{\Delta i(\omega)} = \frac{1}{eV_{\rm a}}\frac{A_{3p}({\rm j}\omega - A_{4q}) + A_{3q}({\rm j}\omega - A_{4q})}{Y_1(\omega)}, \tag{43}$$

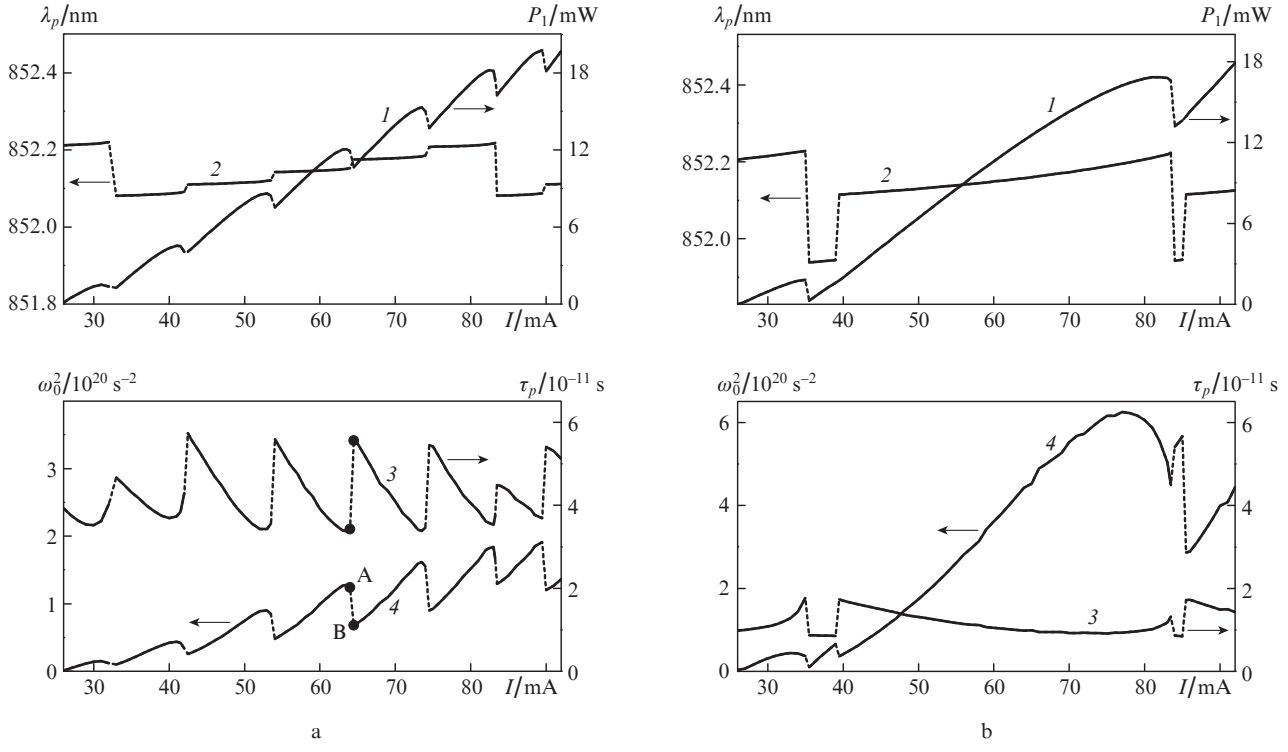

Figure 6. Pump current for a single mode of the FBG LD vs. radiation power P_1 (*1*), radiation wavelength (*2*), lifetime of the photons in the cavity (*3*) and frequency of the relaxation oscillations (*4*) for the fibre lengths L_2 = (a) 7.6 and (b) 1.0 mm.

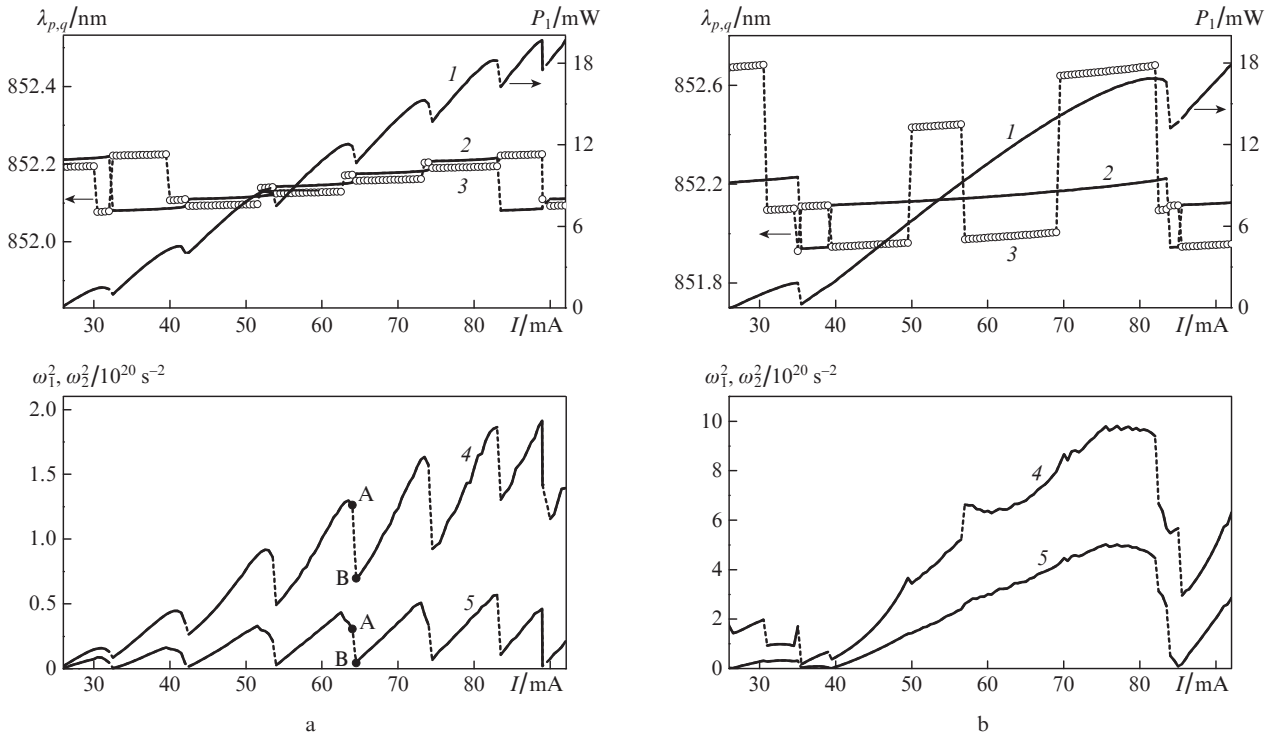

Figure 7. Pump current for two modes of the FBG LD vs. radiation power P_1 (*1*), radiation wavelength λ_p (*2*), radiation wavelength λ_q (*3*), frequency of the relaxation oscillations ω_2^2 (*4*) and frequency of the relaxation oscillations ω_1^2 (*5*) for the fibre lengths L_2 = (a) 7.6 and (b) 1.0 mm.

where $Y_1(\omega)$ is defined by equality (28) and its coefficients – by equality (29).

The normalised AFC can be written as

$$M_2(\omega) = 10\lg\left\{\frac{\omega_1^4[1+(b\omega/a)^2]}{(\omega_1^2-\omega^2)^2+(\omega/A_\Sigma)^2(\omega_2^2-\omega^2)^2}\right\}, \qquad (44)$$

where

$$\begin{aligned}
&\omega_1^2 = (1/A_\Sigma)[(A_1A_{4p} - A_{2p}A_{3p})A_{4q} - A_{2q}A_{3q}A_{4p}],\\
&a = -(A_{3p}A_{4q} + A_{3q}A_{4p}),\ b = A_{3p} + A_{3q},\\
&\omega_2^2 = A_{1p}A_{4p} - A_{2p}A_{3p} + A_{4q}(A_1 + A_{4p}) - A_{2q}A_{3q},\\
&A_\Sigma = A_{1p} + A_{4p} + A_{4q}.
\end{aligned} \qquad (45)$$

Figure 7 shows the pump current as a function of the radiation power P_1, wavelengths λ_p and λ_q, and relaxation oscillation frequencies ω_1^2 and ω_2^2 calculated by using formulas (45) for the fibre lengths L_2 = 7.6 and 1.0 mm.

The results of AFC calculations conducted using formula (44) for the pump current of 60 mA and the fibre lengths of L_2 = 7.6 and 1.0 mm showed their complete agreement with the results of calculations for the single-mode approximation by formula (39). Therefore, to simplify the AFC calculations it is reasonable to use formula (39).

8. Discussion of the results and conclusions

Comparison of the calculated dependences with the experimental plots from [12] for single-mode lasing shows that system (1) and (2b), in which the rate equation for the carriers does not make use of Γ_a, better describes the experiment than system (1) and (2a). In the two-mode case, both systems inadequately describe the experiment.

The FBG LD characteristics calculated for a single mode using formula (32), which does not take into account the radiation power coupled output of the cavity, have no discontinuities inherent in characteristics obtained with P_1 taken into account. The characteristics in the two-mode case also have no discontinuities, but the noise levels for both systems are much greater than the noise level obtained by taking P_1 into account and increase with increasing pump current.

The nonlinearity coefficient (12) varies in the range $(3-4)\times10^{-17}$ cm^3 for system (1) and (2a) and in the range $(3-4)\times10^{-15}$ cm^3 for system (1) and (2b).

Expression (20) for RIN can be transformed into formula (115) from paper [5]. Calculations performed by using both formulas gave the same results.

Expression (30) can be transformed into formula (22) from paper [17]. Calculations performed by using both formulas gave the same results (in this case, F_q should be equal to F_p).

Using Hooge's hypothesis for RIN allowed the theoretical curves to agree with the experimental curves from [12], except for RIN(I) at the pump current ranging from 70 to 73 and from 80 to 95 mA. The reason for the discrepancy is the inability to obtain in theory simultaneous lasing of two modes with approximately equal amplitudes in the calculations based on formula (8), while in the experiment simultaneous lasing of two modes is possible. This may be due to the fact that we do not take into account the reflection of light from the lens, which falls onto the LD, causing additional noise [in the experiment we used an AR-coated ($R < 0.5\%$) two-lens objective and two AR-coated protective glass plates). In addition to the nonlinearity of the gain (12), it is necessary to take into account the nonlinearity associated with the spectral burning of the carriers and carrier transport [9, 10]. We did

not consider the heating of the LD cavity mirrors associated with the radiation absorption in the near-surface region of the crystal, causing local heating of the mirror and the reduction in the band gap, which leads to a further increase in the absorption and the LD crystal temperature rise.

Both systems of the rate equations for the specified current yield identical AFCs in the case of one and two modes.

Shortening the length of the fibre leads to the broadening of the range of continuous tuning of the radiation power and wavelength, to reduction of the photon lifetime in the cavity and to an increase in the resonance frequency.

References

1. Zhuravleva O.V., Ivanov A.V., Leonovich A.I., Kurnosov V.D., Kurnosov K.V., Chernov R.V., Shishkov V.V., Pleshanov S.A. *Kvantovaya Elektron*., **36**, 741 (2006) [*Quantum Electron*., **36**, 741 (2006)].
2. Zhuravleva O.V., Ivanov A.V., Kurnosov V.D., Kurnosov K.V., Mustafin I.R., Simakov V.A., Chernov R.V., Pleshanov S.A. *Kvantovaya Elektron.*, **38**, 319 (2008) [*Quantum Electron*., **38**, 319 (2008)].
3. Ivanov A.V., Kurnosov V.D., Kurnosov K.V., Romantsevich V.I., Chernov R.V., Marmalyuk A.A., Volkov N.A., Zholnerov V.S. *Kvantovaya Elektron.*, **41**, 692 (2011) [*Quantum Electron*., **41**, 692 (2011)].
4. Zholnerov V.S., Ivanov A.V., Kurnosov V.D., Kurnosov K.V., Lobintsov A.V., Romantsevich V.I., Chernov R.V. *Zh. Tekh. Fiz*., **82**, 63 (2012).
5. Yamamoto Y. *IEEE J. Quantum Electron*., **19**, 34 (1983).
6. Marcuse D. *IEEE J. Quantum Electron*., **20**, 1139 (1984).
7. Yamada M. *IEEE J. Quantum Electron*., **22**, 1052 (1986).
8. Agrawal G.P., Dutta N.K. *Long-Wavelength Semiconductor Laser* (New York: Van Nostrand, 1986).
9. Nagarajan R., Ishikawa M., Fukushima T., Geels R.S., Bowers J.E. *IEEE J. Quantum Electron.*, **28**, 1990 (1992).
10. Tsai C.-Y., Shih F.-P., Sung T.-L., Wu T.-Y., Chen C.-H., Tsai C.-Y. *IEEE J. Quantum Electron*., **33**, 2084 (1997).
11. Bogatov A.P. Preprint FIAN No. 256 (Moscow, 1988).
12. Zholnerov V.S., Ivanov A.V., Kurnosov V.D., Kurnosov K.V., Romantsevich V.I., Chernov R.V. *Kvantovaya Elektron*., **43**, 824 (2013) [*Quantum Electron.*, **43**, 824 (2013)].
13. Eliseev P.G. *Vvedenie v fiziku inzhektsionnykh lazerov* (Introduction to Physics of Injection Lasers) (Moscow: Nauka, 1983).
14. Buckingham M.J. *Noise in Electronic Devices and Systems* (Chichester: Ellis Harwood Ltd., 1981; Moscow: Mir, 1986).
15. Garmash I.A., Zverkov M.V., Kornilova N.B., Morozov V.N., et al. Preprint FIAN No. 106 (Moscow, 1989).
16. Bogatov A.P., Eliseev P.G., Kobildzhanov O.A., Madgazin V.R. *IEEE J. Quantum Electron.*, **23**, 1064 (1987).
17. Mukai T., Yamamoto Y. *IEEE J. Quantum Electron.*, **18**, 564 (1982).